

# IndAsT (v1.0) manual

Agustín D. Ruiz López & Katerina Tsiampousi

Geotechnics Section, Department of Civil and Environmental Engineering  
Imperial College London

October 2023

# Contents

<b>1</b>	<b>Introduction</b>	<b>2</b>
<b>2</b>	<b>Formulation of plane-strain beam elements</b>	<b>2</b>
<b>3</b>	<b>Material modelling</b>	<b>4</b>
3.1	Linear elastic model (model 1) . . . . .	5
3.2	Nonlinear model for tunnel joints (model 51) . . . . .	6
<b>4</b>	<b>Outline data file</b>	<b>13</b>
4.1	Compulsory cards . . . . .	13
4.2	Optional cards . . . . .	14
<b>5</b>	<b>Outline mesh file</b>	<b>15</b>
	<b>References</b>	<b>16</b>

# 1 Introduction

IndAsT is a finite element program aimed to the structural analysis of segmental tunnel linings in 2D plane-strain conditions developed in the Geotechnics Section at Imperial College London.

The structural analysis enabled by IndAsT falls within the category of beam-spring analysis where the tunnel is simulated with beam elements and the interaction between the tunnel and the surrounding ground is simulated with normal and, optionally, shear springs. The program enables to introduce non linearity in the analysis through the adoption of a nonlinear model for the longitudinal tunnel joints. Ruiz López et al. (2022) derived a methodology based on the beam-spring approach, using 3D numerical analysis, to derive bending stiffness reduction factors for grey cast iron segmental linings. The primary motivation for the development of IndAsT was to provide a simple tool of analysis that allows this methodology to be implemented in engineering practice.

## 2 Formulation of plane-strain beam elements

The formulation of curved beam elements for plane-strain analysis developed by Day (1990) was implemented in IndAsT. The formulation consists on 3-noded isoparametric finite elements with reduced integration (2-point integration) to alleviate shear locking effects.

The global coordinates  $(x, y)$  of a point within the 3-noded beam with natural coordinates  $(\eta)$  are a function of the element shape functions  $N_i$ :

$$\begin{aligned}x(\eta) &= N_1(\eta)x_1 + N_2(\eta)x_2 + N_3(\eta)x_3 \\y(\eta) &= N_1(\eta)y_1 + N_2(\eta)y_2 + N_3(\eta)y_3\end{aligned}\tag{1}$$

where the subscripts  $i$  indicate the element's local number. Similarly, the global degrees of freedom  $(u, v, \theta)$  at any point within the elements are related to the nodal values according

to the following relationships:

$$\begin{aligned} u(\eta) &= N_1(\eta)u_1 + N_2(\eta)u_2 + N_3(\eta)u_3 \\ v(\eta) &= N_1(\eta)v_1 + N_2(\eta)v_2 + N_3(\eta)v_3 \\ \theta(\eta) &= N_1(\eta)\theta_1 + N_2(\eta)\theta_2 + N_3(\eta)\theta_3 \end{aligned} \quad (2)$$

The shape functions, in natural coordinates, of the 3-noded beam element are defined as follows:

$$\begin{aligned} N_1 &= \frac{1}{2}\eta(\eta - 1), \\ N_2 &= \frac{1}{2}\eta(\eta + 1), \\ N_3 &= (1 - \eta^2) \end{aligned} \quad (3)$$

In turn, the so-called substitute shape functions, see Equation 11, are defined as:

$$\begin{aligned} \bar{N}_1 &= \frac{1}{2}\left(\frac{1}{3} - \eta\right), \\ \bar{N}_2 &= \frac{1}{2}\left(\frac{1}{3} + \eta\right), \\ \bar{N}_3 &= \frac{2}{3} \end{aligned} \quad (4)$$

Day (1990) introduced the following definitions for the strains of the beam element:

$$\begin{aligned} \varepsilon_a &= \cos \alpha \frac{du}{d\eta} + \sin \alpha \frac{dv}{d\eta} \\ \varepsilon_\chi &= -\frac{d\theta}{d\eta} \\ \varepsilon_\gamma &= -\theta - \sin \alpha \frac{du}{d\eta} + \cos \alpha \frac{dv}{d\eta} \end{aligned} \quad (5)$$

where  $\varepsilon_a$  is the axial strain,  $\varepsilon_\chi$  is the bending strain (or curvature) and  $\varepsilon_\gamma$  is the shear strain. Additionally,  $\cos \alpha$  and  $\sin \alpha$  are determined as follows:

$$\sin \alpha = \frac{1}{\det J} \frac{dy}{d\eta} \quad (6)$$

$$\cos \alpha = \frac{1}{\det J} \frac{dx}{d\eta} \quad (7)$$

and where the determinant of the jacobian  $J$  is obtained with the following expression:

$$\det J = \left[ \left( \frac{dx}{d\eta} \right)^2 + \left( \frac{dy}{d\eta} \right)^2 \right]^{\frac{1}{2}} \quad (8)$$

The above definitions of strains (Equation 5) give rise to the definition of the B matrix:

$$\{\varepsilon\} = [B] \cdot \{\delta\} \quad (9)$$

where  $\delta$  is the vector of degrees of freedom. The above expression can be expanded in the following manner:

$$\begin{Bmatrix} \varepsilon_l \\ \chi_l \\ \gamma \end{Bmatrix} = \begin{bmatrix} B_1 \\ B_2 \\ B_3 \end{bmatrix} \cdot \begin{Bmatrix} u_1 \\ v_1 \\ \theta_1 \\ u_2 \\ v_2 \\ \theta_2 \\ u_3 \\ v_3 \\ \theta_3 \end{Bmatrix} \quad (10)$$

$$\begin{bmatrix} B_1 \\ B_2 \\ B_3 \end{bmatrix} = \frac{1}{\det J} \cdot \begin{bmatrix} \cos \alpha \frac{dN_1}{d\eta} & \sin \alpha \frac{dN_1}{d\eta} & 0 & \cos \alpha \frac{dN_2}{d\eta} & \sin \alpha \frac{dN_2}{d\eta} & 0 & \cos \alpha \frac{dN_3}{d\eta} & \sin \alpha \frac{dN_3}{d\eta} & 0 \\ 0 & 0 & \frac{dN_1}{d\eta} & 0 & 0 & \frac{dN_2}{d\eta} & 0 & 0 & \frac{dN_3}{d\eta} \\ -\sin \alpha \frac{dN_1}{d\eta} & \cos \alpha \frac{dN_1}{d\eta} & -\bar{N}_1 & -\sin \alpha \frac{dN_2}{d\eta} & \cos \alpha \frac{dN_2}{d\eta} & -\bar{N}_2 & -\sin \alpha \frac{dN_3}{d\eta} & \cos \alpha \frac{dN_3}{d\eta} & -\bar{N}_3 \end{bmatrix} \quad (11)$$

The element stiffness matrix  $K_e$  is integrated in the natural coordinate system:

$$K_e = \int_{-1}^{+1} B^T D B \det J d\eta \quad (12)$$

where  $D$  is the constitutive matrix, discussed in Section 3.

### 3 Material modelling

At present, two material models for beam elements have been implemented in IndAsT: a linear elastic model, intended to be adopted by tunnel segments and a nonlinear model, intended to simulate the behaviour of the tunnel joints. Table 1 presents the list of material models currently implemented. The formulation and parameters for the two models are introduced in the following sections.

Model number	Model description
1	Linear elastic
51	Nonlinear model for tunnel joints

Table 1: List of material models

### 3.1 Linear elastic model (model 1)

For linear elasticity, the constitutive matrix  $D$ , in plane strain, is established as follows:

$$[D] = \begin{bmatrix} \frac{EA}{1-\mu^2} & 0 & 0 \\ 0 & \frac{EI}{1-\mu^2} & 0 \\ 0 & 0 & \kappa GA \end{bmatrix} \quad (13)$$

where  $E$  is the elastic modulus,  $\mu$  is the Poisson's ratio,  $G$  is the shear modulus,  $\kappa$  is the shear correction factor,  $A$  is the beam's cross-section area (per unit length) and  $I$  is the beam's second moment of area (per unit length). The stress update is simply obtained as:

$$\{\Delta\sigma\} = [D] \cdot \{\Delta\varepsilon\} \quad (14)$$

where  $\Delta$  stands for incremental.

This model requires a total of seven parameters:

P1: 1.0

P2: Unit weight  $\gamma$

P3: Elastic modulus  $E$

P4: Poisson's ratio  $\mu$

P5: Shear correction factor  $\kappa$

P6: Cross-section area  $A$

P7: Second moment of area  $I$

### 3.2 Nonlinear model for tunnel joints (model 51)

The tunnel joint model developed by Ruiz López (2022) has been implemented in In-dAsT. This model describes the nonlinear bending moment-rotation ( $M$ - $\theta$ ) response of the joint for a given axial force  $N$ . It was devised to be adopted by a small beam element representing the joint. Ruiz López (2022) demonstrated that the formulation adopted was capable of representing the rotational behaviour of a wide range of joint geometries; moreover, the results showed that it is possible to simulate the behaviour of a grey cast iron ring with 2D beam elements. A summary of the model formulation is introduced below. In broad terms, the model specifies that the behaviour of the joint prior to joint opening (separation of the segment faces) is linear while thereafter, the model defines the  $M$ - $\theta$  response according to a hyperbolic expression. Note that the formulation is written assuming that compression forces are negative; additionally, the positive and negative signs included as superscripts indicate positive and negative bending, respectively.

The bending moment of opening  $M_o$  is determined from Navier's bending formula assuming linear elasticity. Correspondingly,  $M_o$  is computed as follows for positive bending (i.e. opening at the intrados):

$$M_o^+ = -\frac{N \cdot I}{y_i \cdot A}, \quad (15)$$

similarly, for negative bending (i.e. opening at the intrados):

$$M_o^- = -\frac{N \cdot I}{y_o \cdot A}, \quad (16)$$

where  $y_i$  and  $y_o$  are the distance from the intrados to the centroid and from the extrados to the centroid, respectively. The position of the centroid is calculated by the program from the input dimensions of the joint section ( $b_1$ ,  $h_1$ ,  $b_2$ ,  $h_2$ ,  $b_3$  and  $h_3$ ) which, as shown in Figure 1, allow for general cross-section shape to be adopted.

Figure 2 depicts a graphical representation of the stress state at the onset of opening for both bending modes. It should be noted that the calculation of  $M_o$  assumes that the presence of the joint bolts and their preloading do not influence on the onset of opening, this is in agreement with the outcome from the experimental investigation conducted by Yu (2014). When the axial force  $N$  is tensile, Equations 15 and 16 are ignored and  $M_o$  is taken as zero.

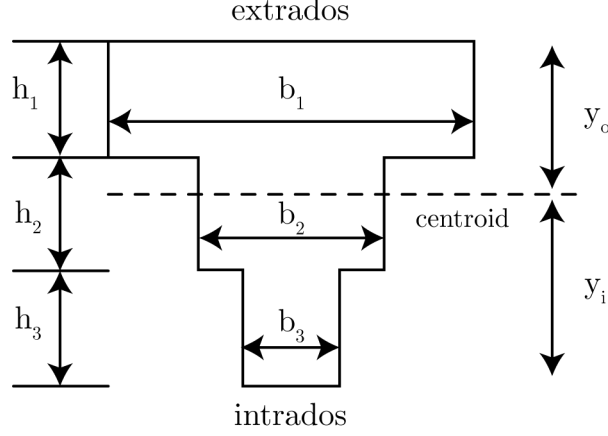


Figure 1: General cross-section dimensions as defined in the joint model

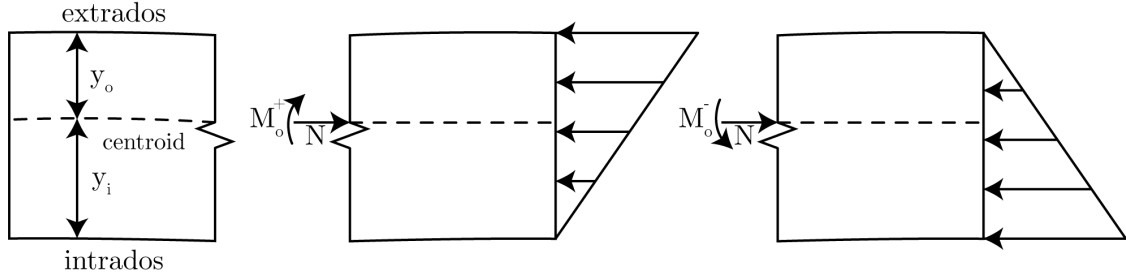


Figure 2: Stress state at the onset of joint opening assumed in the joint model

Prior to opening, the  $M$ - $\theta$  response is governed by the rotational stiffness  $K_o$ . The rotation of the joint can therefore be calculated as follows:

$$\begin{aligned}\theta_o^+ &= \frac{M_o^+}{K_o^+}, \\ \theta_o^- &= \frac{M_o^-}{K_o^-};\end{aligned}\tag{17}$$

When the joint is open ( $M > M_o^+$  or  $-M > M_o^-$ ), the bending moment is defined as:

$$M = M_o + \frac{K_i \cdot (|\theta| - \theta_o)}{\left[1 + \left(\frac{K_i \cdot (|\theta| - \theta_o)}{M_u - M_o}\right)^n\right]^{\frac{1}{n}}},\tag{18}$$

where  $\theta$  is the current rotation,  $K_i$  is the rotational stiffness of the joint at opening and  $n$  is the shape parameter of the  $M$ - $\theta$  curve;  $M_u$  is the ultimate bending moment of the joint. Different parameters  $K_i$  and  $n$  are defined for positive and negative bending such that the expression above is considered separately for both modes. As shown in Figure 3,  $M_u$  is the horizontal asymptote limiting the  $M$ - $\theta$  curve towards which the bending moment  $M$  converges, for a given axial force, with rotation  $\theta$ .



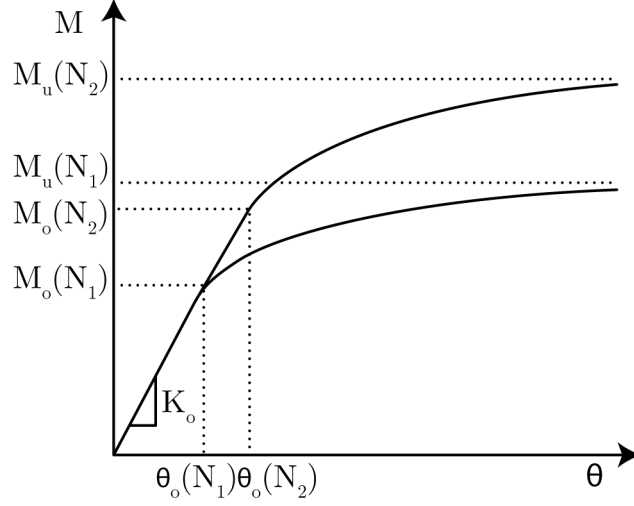


Figure 3: Schematic of the  $M$ - $\theta$  behaviour of the model for different axial force levels

The calculation of the ultimate bending moment  $M_u$  is divided in a tension component  $M_{u,b}$  from the action of the bolts and a compression component  $M_{u,c}$  from the compression force acting at the joint. In line with previous concepts, a distinction is made between the ultimate moment for positive and negative modes. Under positive bending:

$$M_u^+ = M_{u,b} + M_{u,c}^+ \quad (19)$$

The tension component allows for the definition of two rows of bolts at different heights. The calculation of  $M_{u,b}$  assumes that all the bolts reach their tensile strength:

$$M_{u,b} = (n_{b1} \cdot (y_i - h_{G1}) + n_{b2} \cdot (y_i - h_{G2})) \cdot F_{tu,b}, \quad (20)$$

where  $h_{G1}$  and  $h_{G2}$  are the distances from the intrados to the bolt centreline of the first and second row of bolts, respectively;  $n_{b1}$  and  $n_{b2}$  are the number of bolts of the first and second row of bolts, respectively; and  $F_{tu,b}$  is the ultimate tensile force of a single bolt which is determined from:

$$F_{tu,b} = A_b \cdot f_{tu,b} = \frac{\pi \cdot \phi_b^2}{4} \cdot f_{tu,b}, \quad (21)$$

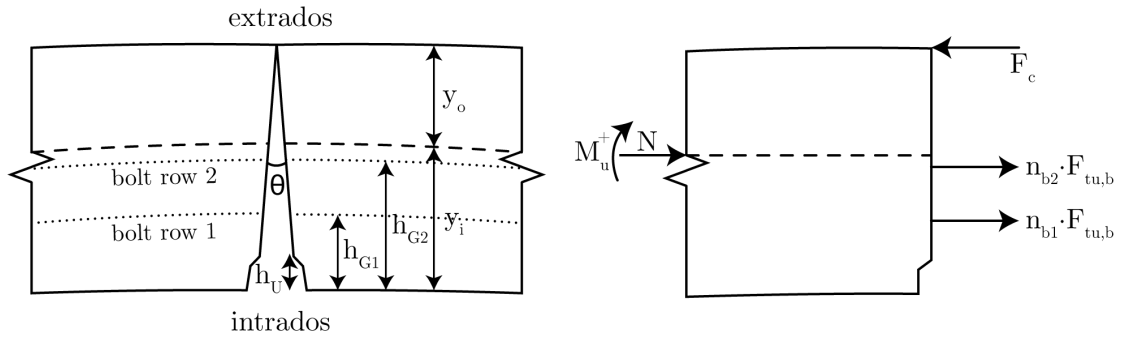
where  $A_b$  and  $\phi_b$  are the bolt thread area and bolt thread diameter, respectively;  $f_{tu,b}$  is the uniaxial tensile strength of the bolt material.

Regarding the compression component  $M_{u,c}$ , the model allows it to be calculated assuming the segment material remains elastic when the joint reaches its ultimate capacity (i.e. contact force acting at the edge of the joint) or, alternatively, considering failure of

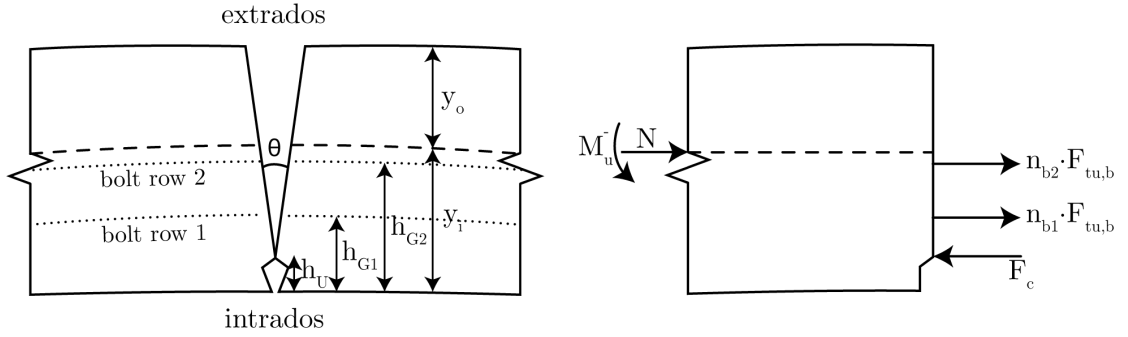
the compressed area. Ruiz López (2022) found in series of 3D numerical analyses that grey cast iron joints generally did not fail in compression and so that the former option is more adequate for this type of tunnel joint. When neglecting failure of the compression area, the compression component for positive bending is determined as follows:

$$M_{u,c}^+ = F_c \cdot y_o = (-N + (n_{b1} + n_{b2}) \cdot F_{tu,b}) \cdot y_o, \quad (22)$$

where  $F_c$  is the contact force, as expanded in the right-hand side of the equality. The stress state at ultimate conditions of a bolted joint for the conditions outlined above is depicted in Figure 4a for positive bending.



(a) Positive bending



(b) Negative bending

Figure 4: Stress state at ultimate capacity of the joint as assumed in the joint model

Similarly to the above, the ultimate moment under negative bending is obtained as follows:

$$M_u^- = -(M_{u,b} + M_{u,c}^-), \quad (23)$$

note that the negative sign in the equation above is adopted for  $M_u^-$  to be a positive quantity. The compression component for negative bending would be:

$$M_{u,c}^- = -F_c \cdot y_i^*, \quad (24)$$

where  $y_i^* = y_i - h_U$ ,  $h_U$  being the depth of the caulking groove, the presence of which in the above equation implies that the caulking groove is not allowed to transmit compressive forces as illustrated in the diagram of forces in Figure 4b.

If the option of accounting for failure in compression is invoked, the height of the caulking groove must be subtracted from the corresponding section dimensions. The height dimensions  $h_1$ ,  $h_2$  and  $h_3$  need to be re-defined according to the value of  $h_U$  as defined below:

$$\begin{aligned}
h_U \leq h_3 \quad \Rightarrow \quad & h_1^* = h_1, \\
& h_2^* = h_2, \\
& h_3^* = h_3 - h_U; \\
h_3 < h_U \leq h_2 + h_3 \quad \Rightarrow \quad & h_1^* = h_1, \\
& h_2^* = h_2 - (h_U - h_3), \\
& h_3^* = 0; \\
h_2 + h_3 < h_U \quad \Rightarrow \quad & h_1^* = h_1 - (h_U - h_2 - h_3), \\
& h_2^* = 0, \\
& h_3^* = 0.
\end{aligned} \tag{25}$$

The ultimate moment  $M_u$  can now be determined in terms of the defined variables  $h_1^*$ ,  $h_2^*$ ,  $h_3^*$  and  $y_i^*$  such that the capacity calculation takes into account the reduced contact area. Clearly, the most compressive axial force allowed by the model is:

$$N_{cu} = -f_c \cdot A^* = -f_c \cdot (b_1 \cdot h_1^* + b_2 \cdot h_2^* + b_3 \cdot h_3^*). \tag{26}$$

where  $f_c$  is the compressive strength of the tunnel lining material. The equations for  $M_u^+$  and  $M_u^-$  are presented below for a non-bolted joint  $F_c = -N$ . Under positive bending: if  $F_c \leq (b_1 h_1^* f_c)$ :

$$M_u^+ = F_c \left( y_o - \frac{F_c}{2b_1 f_c} \right), \tag{27}$$

else if  $(b_1 h_1^* f_c) < F_c \leq (b_1 h_1^* f_c + b_2 h_2^* f_c)$ :

$$M_u^+ = b_1 h_1^* f_c \left( y_o - \frac{h_1^*}{2} \right) + (F_c - b_1 h_1^* f_c) \cdot \left( y_o - \frac{h_1^*}{2} - \frac{(F_c - (b_1 - b_2) h_1^* f_c)}{2b_2 f_c} \right), \tag{28}$$

else  $(b_1 h_1^* f_c + b_2 h_2^* f_c) < F_c$ :

$$\begin{aligned}
M_u^+ = & b_1 h_1^* f_c \left( y_o - \frac{h_1^*}{2} \right) + b_2 h_2^* f_c \left( y_o - \frac{h_1^*}{2} - \frac{h_2^*}{2} \right) + (F_c - (b_1 h_1^* + b_2 h_2^*) f_c) \\
& \cdot \left( y_o - \frac{h_1^*}{2} - \frac{h_2^*}{2} - \frac{F_c - (b_1 h_1^* + b_2 h_2^* - b_3 (h_1^* + h_2^*)) f_c}{2b_3 f_c} \right).
\end{aligned} \tag{29}$$

Similarly, under negative bending:

if  $F_c \leq (b_3 h_3^* f_c)$ :

$$M_u^- = F_c \left( y_i^* - \frac{F_c}{2b_3 f_c} \right), \quad (30)$$

else if  $(b_3 h_3^* f_c) < F_c \leq (b_3 h_3^* f_c + b_2 h_2^* f_c)$ :

$$M_u^- = b_3 h_3^* f_c \left( y_i^* - \frac{h_3^*}{2} \right) + (F_c - b_3 h_3^* f_c) \cdot \left( y_i^* - \frac{h_3^*}{2} - \frac{(F_c - (b_3 - b_2) h_3^* f_c)}{2b_2 f_c} \right), \quad (31)$$

else  $(b_3 h_3^* f_c + b_2 h_2^* f_c) < F_c$ :

$$M_u^- = b_3 h_3^* f_c \left( y_i^* - \frac{h_3^*}{2} \right) + b_2 h_2^* f_c \left( y_i^* - h_3^* - \frac{h_2^*}{2} \right) + (F_c - (b_3 h_3^* + b_2 h_2^*) f_c) \cdot \left( y_i^* - \frac{h_3^*}{2} - \frac{h_2^*}{2} - \frac{F_c - (b_3 h_3^* + b_2 h_2^* - b_1 (h_3^* + h_2^*)) f_c}{2b_1 f_c} \right). \quad (32)$$

Due to the presence of the bolts, the joint section can sustain tensile axial forces, the maximum tensile axial force  $N_{tu}$  is the force resultant of the bolts included in the joint at their ultimate tensile capacity:

$$N_{tu} = (n_{b1} + n_{b2}) \cdot F_{tu,b}. \quad (33)$$

As described above, the model assumes that all the bolts in the joint reach their tensile strength in the calculation of the ultimate moment  $M_u$ . This assumption implies that the lining material does not fail in tension. However, the 3D numerical analyses on a grey cast iron joint performed by Ruiz López (2022) showed that under positive bending a fracture can develop, particularly for the running tunnel geometries, in the circumferential flange or the skin near the end plate before all the bolts fail. For this reason, the option to consider a bending moment cut-off was included in the model. The cut-off is defined via the rotation  $\theta_f$  at which the flange fails in tension, such that, the bending moment does not increase beyond the value  $M_f$ :

$$M_f = M_o + \frac{K_i \cdot (|\theta_f| - \theta_o)}{\left[ 1 + \left( \frac{K_i \cdot (|\theta_f| - \theta_o)}{M_u - M_o} \right)^n \right]^{\frac{1}{n}}}. \quad (34)$$

This model feature is described schematically in Figure 5.

This model requires a total of seven parameters:

P1: 51.0

P2: Elastic modulus  $E$  ( $> 0$ )

P3: Compressive strength  $f_c$  of the tunnel lining material ( $> 0$ ). If  $= -1$ , compressive

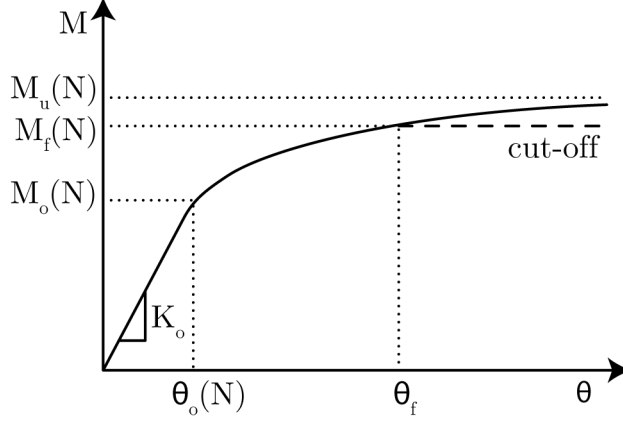


Figure 5: Schematic of the nonlinear  $M$ - $\theta$  response of the model

failure is neglected

P4: Shear modulus  $G$  ( $> 0$ )

P5: Rotational stiffness closed joint under positive bending  $K_o^+$  ( $> 0$ )

P6: Rotational stiffness closed joint under positive bending  $K_i^+$  ( $> 0$ ,  $K_i^+ \leq K_o^+$ )

P7: Shape parameter under positive bending  $n^+$  ( $> 0$ )

P8: Rotational stiffness closed joint under negative bending  $K_o^-$  ( $> 0$ )

P9: Rotational stiffness closed joint under negative bending  $K_i^-$  ( $> 0$ ,  $K_i^- \leq K_o^-$ )

P10: Shape parameter under negative bending  $n^-$  ( $> 0$ )

P11: Number of bolts (per ring) in row bolt 1  $n_{b1}$  ( $\geq 0$ )

P12: Distance from intrados to centre of bolt hole of bolt row 1  $h_{G1}$  ( $h_{G1} - h_U - 0.5\phi_b \geq 0$ ,  $h_1 + h_2 + h_3 - h_{G1} - 0.5\phi_b > 0$ )

P13: Number of bolts (per ring) in row bolt 2  $n_{b2}$  ( $\geq 0$ )

P14: Distance from intrados to centre of bolt hole of bolt row 2  $h_{G2}$  ( $h_{G2} - h_U - 0.5\phi_b \geq 0$ ,  $h_1 + h_2 + h_3 - h_{G2} - 0.5\phi_b > 0$ )

P15: Uniaxial tensile strength of bolts  $f_{tu,b}$  ( $> 0$ )

P16: Diameter of bolt thread  $\phi_b$  ( $> 0$ )

P17: Depth of caulking groove  $h_U$  ( $\geq 0$ )

P18: Geometric dimension (per ring)  $b_1$  ( $\geq 0$ )

P19: Geometric dimension  $h_1$  ( $\geq 0$ )

P20: Geometric dimension (per ring)  $b_2$  ( $\geq 0$ )

P21: Geometric dimension  $h_2$  ( $\geq 0$ )

P22: Geometric dimension (per ring)  $b_3$  ( $\geq 0$ )

P23: Geometric dimension  $h_3$  ( $\geq 0$ )

P24: Joint rotation (in degrees)  $\theta_f^+$  corresponding to  $M_f^+$  ( $\geq 0$ )

P25: Joint rotation (in degrees)  $\theta_f^-$  corresponding to  $M_f^-$  ( $\geq 0$ )

## 4 Outline data file

The program will raise an error if empty lines are included, between the # symbols at the beginning and ends of the data file. Additionally, the user must be careful about leaving any spacing at the end of the lines as this will also trigger an error.

### 4.1 Compulsory cards

#### Mesh card

#MESH filename.msh

#### Final increment

#FINAL INCREMENT P1

P1: integer indicating the total number of analysis increments

#### Dimension

#DIMENSION P1

P1 1 -2D plane stress (not implemented yet)

2 - 2D plane strain

3 - 2D axisymmetry (not implemented yet)

4 - 3D (not implemented yet)

#### Integration

#INTEGRATION P1

P1 1 - Full integration

2 - Reduced integration

#### Linear elastic properties

#LINEAR ELASTIC PROPERTIES

"Material" material\_number P1 ...

#### Nonlinear elastic properties

#NONLINEAR ELASTIC PROPERTIES

"Material" material\_number P1 ...

if the material does not adopt nonlinear elasticity then  $P1=0.0$

## 4.2 Optional cards

### Prescribed displacements

#PRESCRIBED DISPLACEMENTS

"Nodes" set\_number node1 ...

"Component" set\_number P1

"Displacement" set\_number magnitude

"Increments" set\_number increment\_n increment\_n1 ...

P1 1 - Displacement x-direction

2 - Displacement y-direction

3 - Rotation

if increment\_n=-1, then the displacement/rotation constraint is imposed in all increments of the analysis.

### Point loads

#POINT LOADS

"Nodes" set\_number node1 ...

"Component" set\_number P1

"Magnitude" set\_number magnitude

"Increments" set\_number increment\_n increment\_n1 ...

P1 1 - Load x-direction

2 - Load y-direction

3 - Bending moment

if increment\_n=-1, then the point load is imposed in all increments of the analysis.

### Graph output

#GRAPH OUTPUT

"Nodes" set\_number node1 ...

"Component" set\_number P1

"Inc\_N" set\_number increment\_n increment\_n1 ...

```

P1  1 - Displacement x-direction
    2 - Displacement y-direction
    3 - Rotation
"Elements" set_number element1 ...
"Int_Pt" set_number gp1 ...
"Component_IP" set_number P1
"Inc_Pt" set_number increment_n increment_n1 ...
P1  1 - Axial force
    2 - Bending moment
    3 - Shear force

```

### **Contour plot output (GID format)**

```

#GID OUTPUT
"Increments" increment_n increment_n1 ...

```

if increment\_n=-1, then the point load is imposed in all increments of the analysis.

## **5 Outline mesh file**

```

"MESH dimension 2 ElemType Beam Nnode 3"
"Coordinates"
1 x_coord1 y_coord1
2 x_coord2 y_coord2
...
"End Coordinates"
"Elements"
1 node1 node2 node3 mat_number
2 node1 node2 node3 mat_number
...
"End Elements"

```



## References

- Day, R. A. (1990). *Finite element analysis of sheet pile retaining walls*. PhD thesis, Imperial College London (University of London).
- Ruiz López, A., Tsiamposi, A., Standing, J. R., and Potts, D. M. (2022). Numerical investigation of a segmental grey cast iron tunnel ring: validation with laboratory data and application to field conditions. *Computers and Geotechnics*, 141:104427.
- Ruiz López, A. D. (2022). *Development of advanced numerical models for grey cast iron tunnel linings*. PhD thesis, Imperial College London.
- Yu, J. B. Y. (2014). *Assessing ground interaction effects and potential damage on existing tunnels before and after new excavation works*. PhD thesis, Imperial College London.